Electronic Supplementary Material (ESI) for Nanoscale.
This journal is © The Royal Society of Chemistry 2021

Electronic Supplementary Information

Exploiting cyanine dye J-aggregates/monomer equilibrium in hydrophobic protein pockets for efficient multi-step phototherapy: An innovative concept for smart nanotheranostics

Matías L. Picchio[1], Julian Bergueiro[2,3], Stefanie Wedepohl[2], Roque J. Minari[4], Cecilia I. Alvarez Igarzabal[1], Luis M. Gugliotta[4], Julio C. Cuggino[4*] and Marcelo Calderón[5,6*]

[1)] *Departamento de Química Orgánica, Facultad de Ciencias Químicas, Universidad Nacional de Córdoba, IPQA, CONICET-UNC, Haya de la Torre y Medina Allende. Ciudad Universitaria. Córdoba (X5000 HUA) Argentina.*

[2)] *Freie Universität Berlin, Institut für Chemie und Biochemie, Takustrasse 3, 14195 Berlin, Germany*

[3)] *Centro Singular de Investigación en Química Biolóxica e Materiais Moleculares (CiQUS), Departamento de Química Orgánica, Universidade Santiago de Compostela, Spain*

[4)] *Instituto de Desarrollo Tecnológico para la Industria Química (INTEC), CONICET-UNL. Güemes 3450. Santa Fe (3000) Argentina.*

[5)] *POLYMAT, Applied Chemistry Department, Faculty of Chemistry, University of the Basque Country UPV/EHU, Paseo Manuel de Lardizabal 3, 20018 Donostia-San Sebastián, Spain*

[6)] *IKERBASQUE, Basque Foundation for Science, 48009 Bilbao, Spain.*

*Corresponding authors:

Prof. Dr. Marcelo Calderón

Email: marcelo.calderon@polymat.eu

Dr. Julio C. Cuggino

Email: jcuggino@intec.unl.edu.ar

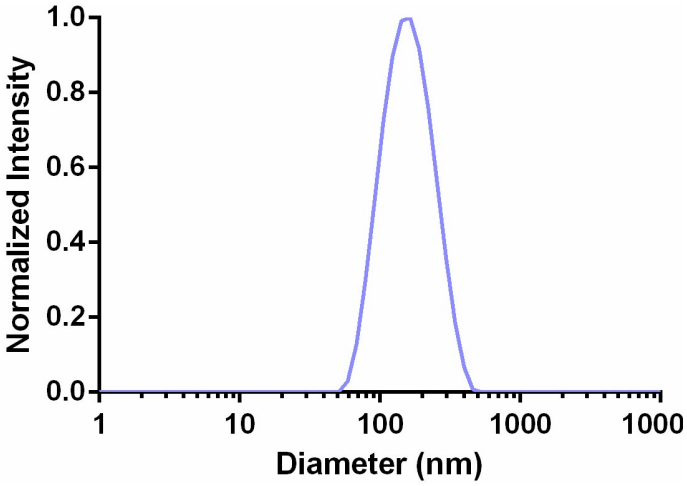

Figure S1. Particle size distribution of casein micelles re-assembled by Ca^{+2}/phosphoserine ionic binding.

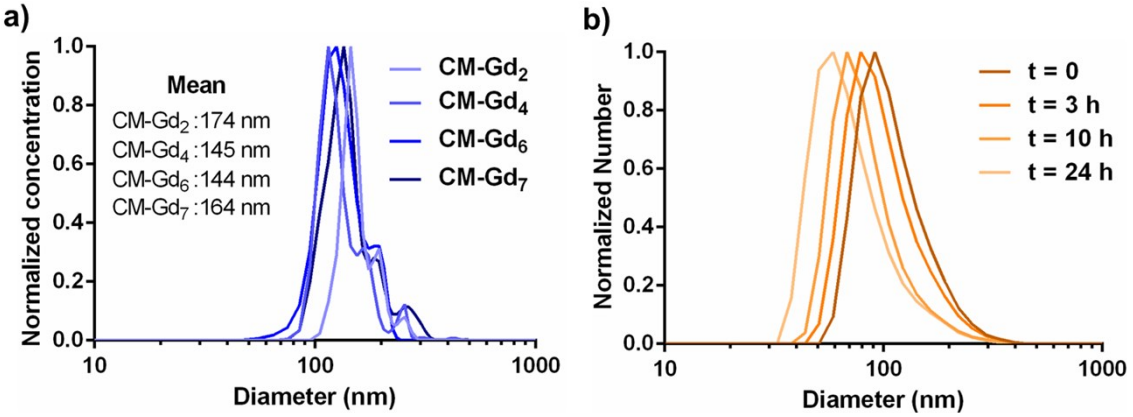

Figure S2. (a) Number weighted size distribution of CM-Gd_x determined by NTA. (b) Number weighted size distribution by DLS of CM-Gd_7 over time upon cathepsin B addition. Maximum peak at 91.3, 78.8, 68.0, and 57.8 nm for 0, 3, 10 and 24 h, respectively.

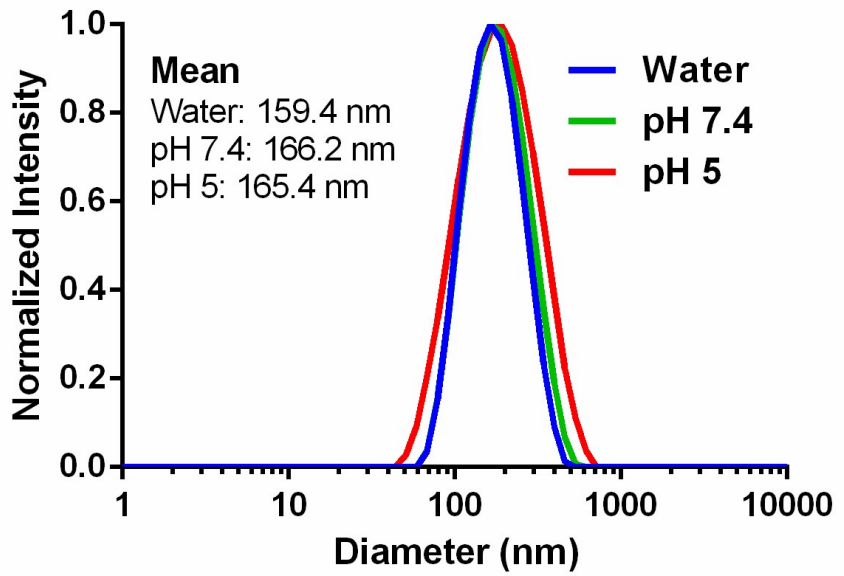

Figure S3. Colloidal stability of CM-Gd_7-J-ICG measured as size distributions in different media. The dye concentration was 15 wt.% based on micelles.

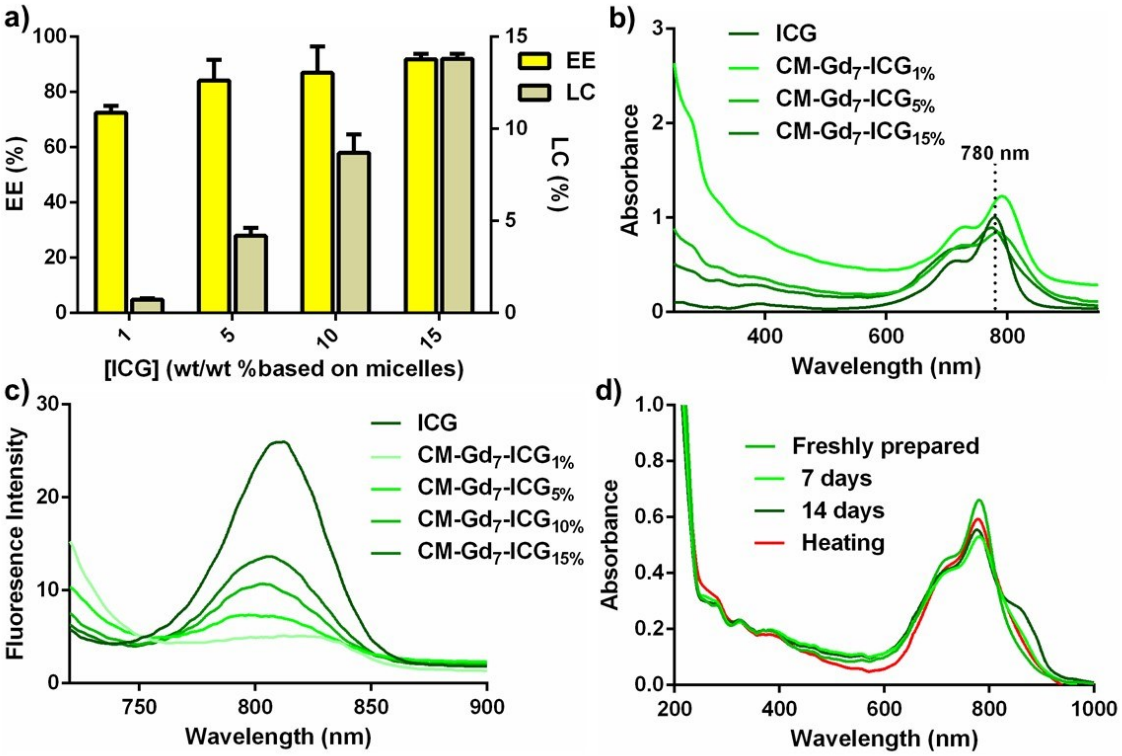

Figure S4. (a) Encapsulation efficiency (EE) and loading capacity (LC) of ICG in CM-Gd_7 for different micelles/dye ratios. (b) UV and (c) fluorescence spectra of ICG and CM-Gd_7-ICG for different dye concentrations. (d) Evolution of UV spectra of CM-Gd_7-ICG at the concentration of 1.2 mg/mL for freshly prepared sample, after ageing for 7

and 14 days at 4 °C, and after heating at 65 °C for 24 h. The samples were diluted to a dye concentration of 5 μg/mL prior analysis.

Figure S4a shows the encapsulation efficiency and loading capacity of ICG in CM-Gd_7 micelles. As it can be seen, micelles were able to encapsulate high amounts of dye (more than 1 mg/mL), indicating good interaction between both components. In fact, UV-visible analysis showed a significant red shift in the characteristic absorption peak of ICG when it was encapsulated (Figure S4b). This result indicates that the microstructure of ICG is considerably affected by its strong binding with casein within the micelles. Fluorescence measurements obtained further evidence of the effective ICG encapsulation. As shown in Figure S4c, a decrease in the fluorescence intensity was observed for CM-Gd_7-ICG compared with free ICG. This behavior is probably due to the concentration of ICG into the micelles' core, causing self-quenching to reduce the fluorescence quantum yields of the dye.

After the ICG encapsulation, we evaluated the *in situ* formation of J-ICG within the micelles. Interestingly, we found out that the aggregate form was not obtained even after ageing CM-Gd_7-ICG for 14 days at 4 °C, only observing a small shoulder around 850 nm (Figure S4d). Even more, J-aggregates were not formed after CM-Gd_7-ICG heating at 65 °C for 24 h. These results suggest that the stabilization of ICG in the micelles and the strong ICG-protein binding could hamper the dye's self-assembled.

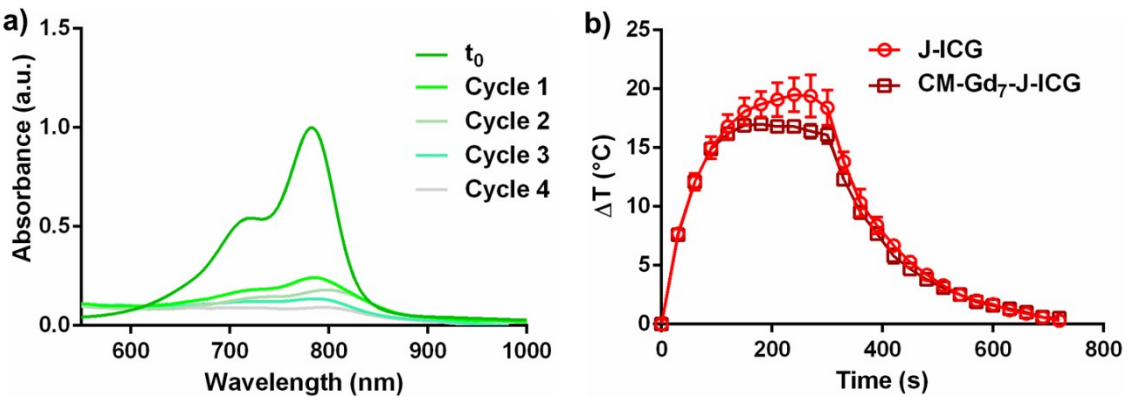

Figure S5. (a) Evolution of UV-visible spectra of ICG after four laser ON/OFF cycles. (b) Steady-state heating curve for J-ICG and CM-Gd_7-J-ICG photothermal agents at 5 μg/mL.

Calculation of photothermal conversion efficiency (η)

$$\eta = \frac{hA(T_{max} - T_{surr}) - Q_{in,\,surr}}{I(1 - 10^{-A_\lambda})}$$

(Eq. S1)

Where h is the heat transfer coefficient, A is the surface area of the container, T_{max} is the maximum steady-state temperature, T_{surr} is the ambient surrounding temperature, I is the laser power (500 mW), A_λ is the absorbance at the excitation wavelength of 785 nm (1.68 AU, from Figure S1b). $Q_{in,surr}$ is the heat input due to light absorption by the water medium (3.25 mW). The quantity hA was calculated as follows:

$$hA = \frac{m_w Cp_w}{\tau_s}$$

Where m_w and Cp_w are the mass and specific heat capacity of the water medium and τ_s was calculated by measuring the rate of temperature drop after removing the laser source (Figure S5b), from the following equations:

$$t = -\tau_s ln\theta$$

$$\theta = \frac{T - T_{surr}}{T_{max} - T_{surr}}$$

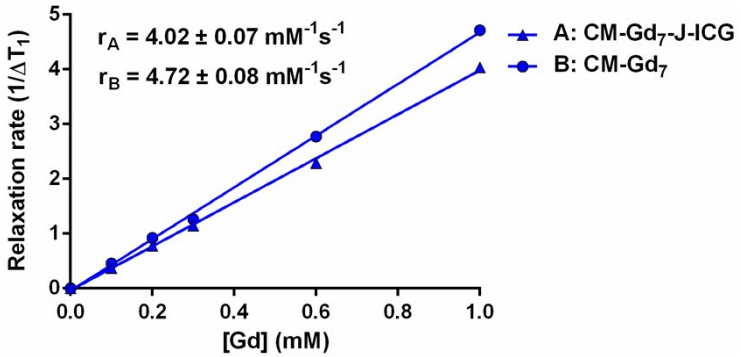

Figure S6. T_1 relaxivity (r_1) for CM-Gd_7-J-ICG (r_A) and CM-Gd_7 (r_B).

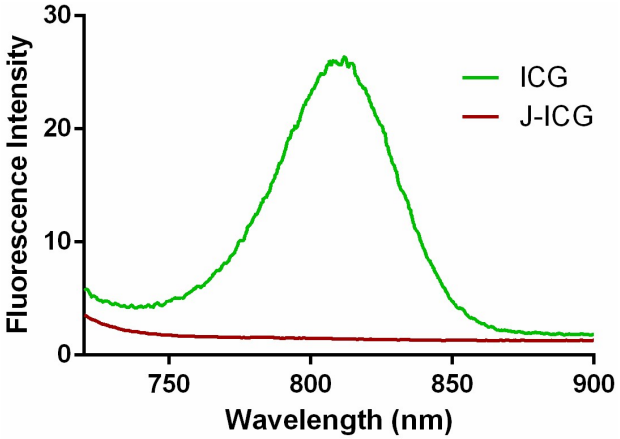

Figure S7. Fluorescence spectra of ICG and J-ICG at a dye concentration of 10 µg/mL.

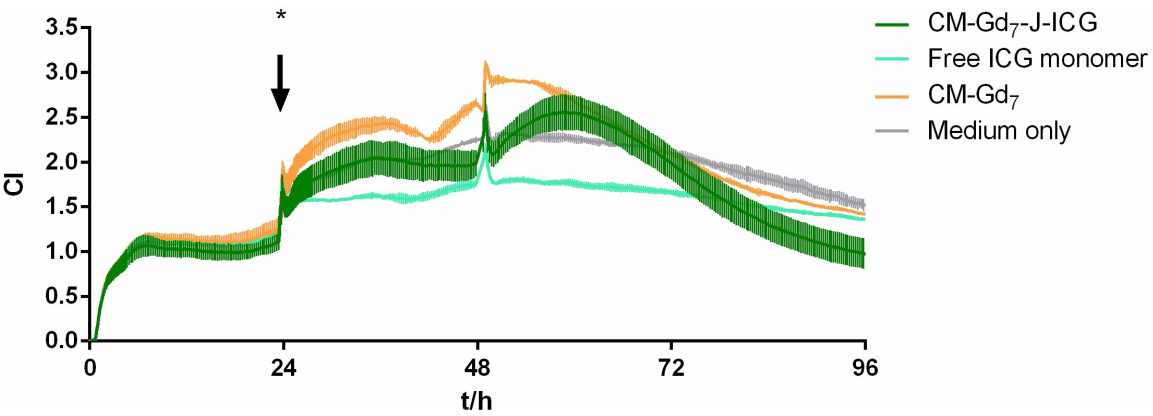

Figure S8. Real-time cell analysis of HeLa cells incubated with CM-Gd_7-J-ICG, free ICG monomer, CM-Gd_7, and medium only, control experiment *without* NIR irradiation. The asterisk denotes the time point of addition of the compounds after 24h. After 48h,

the plate was removed and handled in parallel to the irradiated plate (see Figure 6, main manuscript).

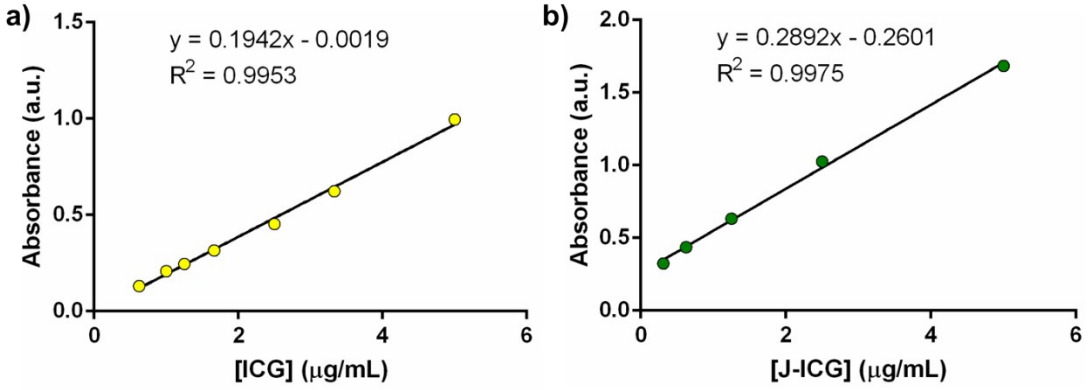

Figure S9. Calibration curve for the absorbance at 780 and 895 nm versus concentration of ICG (a) and J-ICG (b) in water.